

# Fatigue Performance Evaluation for Welded Details in Orthotropic Steel Deck Bridges Using Multi-Scale Finite Element Method

Rongfeng Chen<sup>1</sup> and Changqing Miao<sup>2,\*</sup>

<sup>1</sup>Key Laboratory of Concrete and Prestressed Concrete Structure of Ministry of Education, Southeast University, Nanjing, 210000, China

<sup>2</sup>School of Civil Engineering, Southeast University, Nanjing, 210000, China

\*Corresponding Author: Changqing Miao. Email: chqmiao@seu.edu.cn

Received: 31 October 2019; Accepted: 01 April 2020

**Abstract:** In order to study the fatigue properties of rib-to-deck welded connection and rib-to-rib welded connection in orthotropic steel bridge decks, a multi-scale finite element model was set up to analyze the stress distribution characteristics and the load test was conducted on the Taizhou Yangtze River Bridge. Comparing the vehicle test results with the multi-scale finite element model results to verify the accuracy of the finite element simulation for the stress response of two welded details. The results indicated that: The stress at the rib-to-deck welded connection and the rib-to-rib welded connection are the bending stress and the membrane stress, respectively; the stress response of the two welded connection has strong local characteristics; the lateral stress influence line of the two welded connection is relatively short and the length of the lateral stress influence line is greatly affected by the longitudinal ribs; increasing the thickness of the roof and longitudinal ribs can reduce the stress response and improve the stress performance of the heavy lanes. For the two welded details, the fatigue damage increment of the ordinary lane is greater than the heavy lane. The thickened roof and longitudinal ribs at the position of the heavy lane still cannot balance the fatigue damage caused by the heavy truck. Therefore, it is necessary to strictly control the fatigue effect of overloaded vehicles on steel box girders.

**Keywords:** Orthotropic steel bridge decks; welded details; multi-scale finite element model; load test

## 1 Introduction

Orthotropic steel bridge decks (OSDs) are the most widely used in long-span highway bridges as the main structure of steel box girders with the merits of lighter weight, few welds, and structural redundancy [1–5]. However, the fatigue cracking problem of the welds in steel box girders under vehicle loads is more prominent due to the complicated structure of the orthotropic steel bridge deck [6–10].

In recent years, scholars have gradually realized the fatigue problem of orthotropic steel bridge decks. Zhang et al. [11] systematically sorted out the fatigue problem, fatigue characteristics and evaluation method of the current orthotropic steel bridge deck, and analyzed the new structure of the orthotropic steel bridge



This work is licensed under a Creative Commons Attribution 4.0 International License, which permits unrestricted use, distribution, and reproduction in any medium, provided the original work is properly cited.

deck. Connor et al. [12] discussed the fatigue problem of the OSDs from the aspects of manufacturing, testing, inspection, evaluation and maintenance. In order to accurately predict the fatigue damage of steel box girder and establish a perfect anti-fatigue design analysis method, many scholars have carried out plenty of research work [13–16].

At present, scholars have made great progress in the research of orthotropic steel bridge decks. Liu et al. [17] took Hong Kong-Zhuhai-Macao Bridge as an example, and established the numerical simulation method for crack propagation of U-rib butt welds in orthotropic steel deck based on linear elastic fracture theory. The effectiveness and feasibility of numerical simulation method is verified by model test. A lot of research has been devoted to evaluation of fatigue damage of OSDs under traffic loads by the finite element models [18,19] and experiments [20,21]. Cheng et al. [22] studied the fatigue cracking process, fatigue characteristics and fatigue mechanism of the rib welded connection under cyclic loading through the fatigue test. Deng et al. [23] proposed a time-dependent fatigue reliability assessment approach for welded details of orthotropic steel decks (OSDs) using long-term strain monitoring data. Zhu et al. [24] established the real bridge's finite element model based numerical simulation method and proposed the process of fatigue crack growth of orthotropic steel bridge deck to investigate the fatigue crack growth process of orthotropic steel bridge deck. Mustafa et al. [25] compared the results of the finite element calculations with the results of the fatigue tests which were carried out on full-scale specimens, and the results of the finite element analyses revealed that the structural hot spot stresses obtained from the shell element models were unrealistically high when the welds were omitted.

It can be seen that the research method which focuses on the structural details of the orthotropic steel bridge deck and the fatigue performance of the welded details by fatigue test is a common research method, and the mechanical performance of the orthotropic steel bridge deck structure can be determined, and the fatigue life of the bridge can be evaluated. In order to ensure the safety of the bridge during its service, this research has important engineering practical value.

In this paper, a multi-scale finite element model is established to study the stress response of different bridge decks with the aim of determining the most unfavorable lane according to the investigation of vehicle load on different lanes. Then the orthotropic steel bridge deck model was established to study the stress characteristics of the rib-to-deck welded connection and rib-to-rib welded connection, and then the load test was carried out on the Taizhou Yangtze River Bridge. Finally, the load test result was compared with the multi-scale finite element model result. The accuracy of the finite element model to simulate the stress response of two welded details was verified.

## **2 Engineering Background and Multi-Scale Finite Element Model**

### ***2.1 Engineering Background***

The Taizhou Yangtze River Bridge is located between the Jiangyin Yangtze River Bridge and the Runyang Yangtze River Bridge. The main bridge which adopts the form of three-tower and two-span continuous steel box girder suspension bridge is  $2 \times 1080$  m long. The main cable span is  $390 \text{ m} + 2 \times 1080 \text{ m} + 390 \text{ m}$  long. The main beam is 3.5 m high, 39.10 m wide and 16 m long. Fig. 1 shows the profile of Taizhou Yangtze River Bridge.

The main beam of Taizhou Yangtze River Bridge is full-welded streamlined flat steel box girder structure. The upper and lower flanges adopt orthogonal orthotropic plate structure, and U-shaped ribs are used to strengthen the out-of-plane stiffness of the upper and lower decks. The diaphragm is used to enhance the integrity of the flat steel box girder and the local stiffness of the upper and lower decks. Figs. 2 and 3 show the standard section of the flat steel box girder of the Taizhou Yangtze River Bridge.

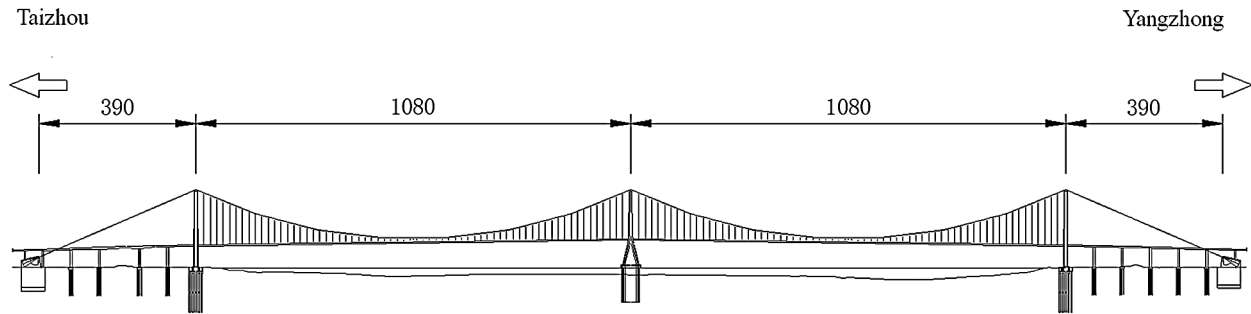


**Figure 1:** Profile of Taizhou Yangtze River Bridge (dimensions in m)

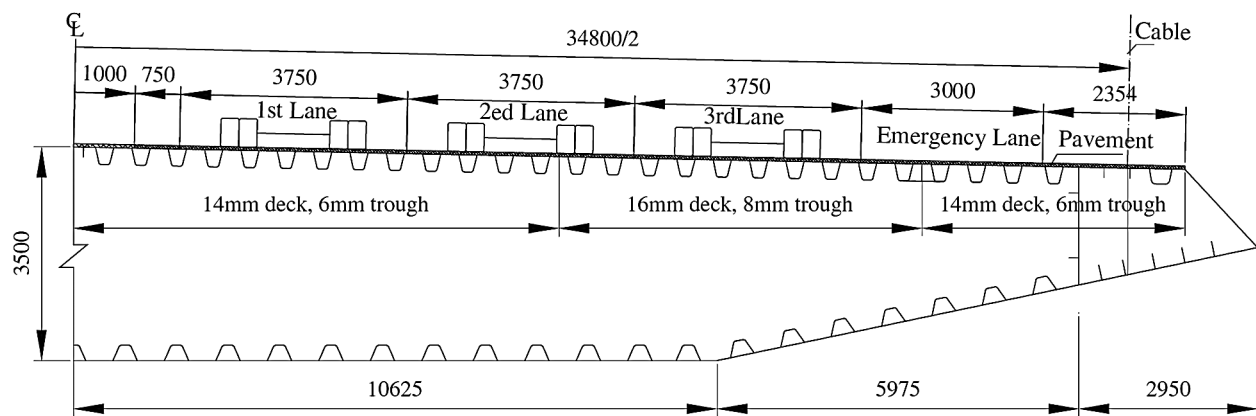


**Figure 2:** Local cross section diagram

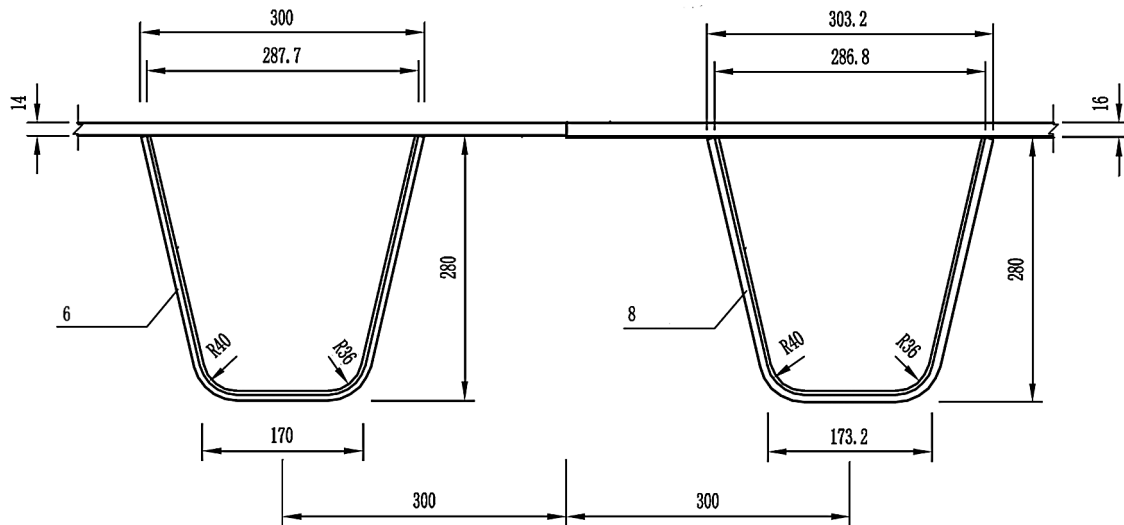


**Figure 3:** The top plate and U-rib structure diagram

### 2.2 Multi-Scale Finite Element Model

In order to obtain the stress response of the bridge deck, the sub-model method is adopted in this paper: firstly, the large-scale model of the whole structure is established, then the local refined model of the steel box girder is established, and finally the local refined model is effectively connected with the overall model.

Embed a small-scale model into a large-scale model and then analyze it, which not only ensures the accuracy of the calculation, but also improves the computational efficiency.

### 2.2.1 Large-Scale Model

In the finite element software ANSYS, the main girder is simulated by the “spine beam” of single main beam, and the main beam is simulated by Beam4. The main cable and boom of the suspension bridge are simulated by Link10. The simulation of the tower can be simplified to a three-dimensional solid beam, which is simulated by Beam4. Fig. 4 shows the large-scale model of the Taizhou Yangtze River Bridge.

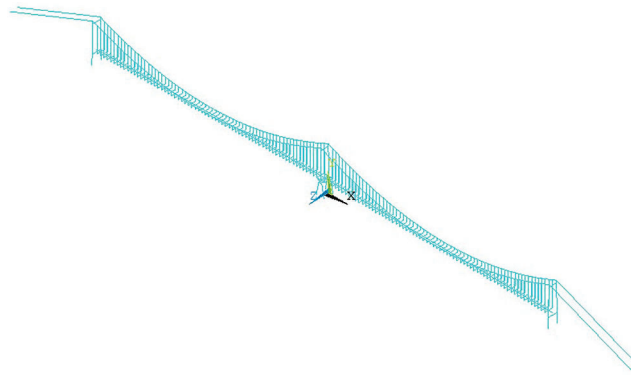


**Figure 4:** The large-scale model of the Taizhou Yangtze River Bridge

The large-scale model is calculated in the software ANSYS, and the vibration parameters which reflect the innate property of the bridge model is obtained. The parameters from ANSYS are compared with that from test which conducted when the bridge construction is completed. Tab. 1 shows the result of the comparison.

**Table 1:** The comparative result of vibration parameter

Vibration mode	Model result	Test result	Relative error (%)
1	0.08443	0.0915	7.7
2	0.08491	0.0808	-5.1
3	0.10678	0.1053	-1.4
4	0.11435	0.1190	3.9
5	0.11719	0.1202	2.5

It can be concluded from Tab. 1 that the low order frequency of vibration mode from ANSYS model relatively correspond to that from bridge test, which indicates that the “spine beam” model can accurately calculate the global response of the bridge. Hence, it can be obtained that the large-scale model is proper enough to simulate the real bridge.

### 2.2.2 Local Refined Model of Steel Box Girder Segment

The statistics of the real bridge show that the fatigue effect of the steel box girder at the position of the first boom on the left and right sides of the middle tower is the most obvious, which is the key part of fatigue analysis. According to the steel box girder design drawing (shown in Figs. 2 and 3), the refined finite element model of the steel box girder within 72 m near the steel middle tower established by the Shell63 unit is shown in Fig. 5.

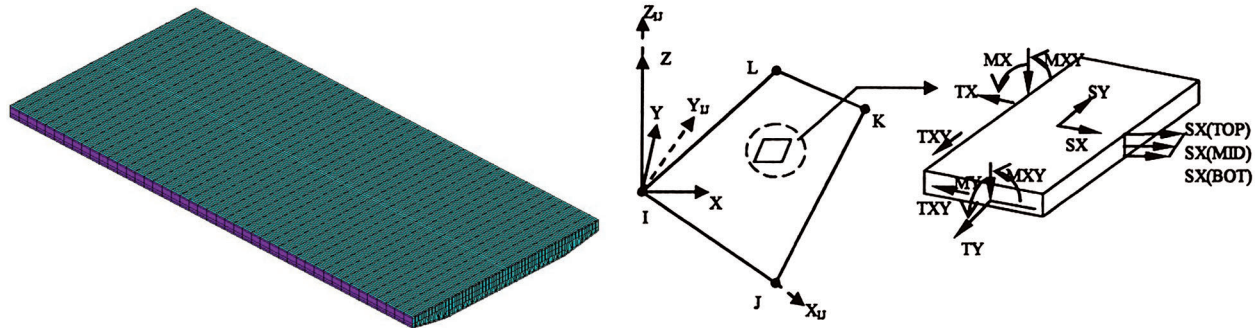


**Figure 5:** The refined finite element model of the steel box girder and shell63 unit

The shell element has  $n$  nodes at the interface, the interface between the beam and the shell element is shown in Fig. 6. The displacement of each node in the overall coordinate system of the structure is:

$$\{\delta_i\} = \{u_i \ v_i \ w_i \ \theta_{xi} \ \theta_{yi} \ \theta_{zi}\} \quad (1)$$

In order to ensure the displacement coordination at the interface, the node displacement of the beam element has a certain relationship with the node displacement of the plate element. The first is the rigid body translation so that the displacement of each node on the interface satisfies the following formula:

$$u = u_i \quad v = v_i \quad w = w_i \quad (2)$$

When the joint is rotated around the  $x$ -axis, the displacement increment of the node  $i$  in the  $y$  and  $z$  directions is:

$$\left. \begin{aligned} \Delta v &= -\rho_i [\sin \alpha_i - \sin(\alpha_i - \theta_x)] \\ \Delta w &= \rho_i [\cos(\alpha_i - \theta_x) - \cos \alpha_i] \end{aligned} \right\} \quad (3)$$

In the formula,  $\rho_i$  is the distance from the shell node  $i$  to the beam node 2 at the interface.

When the joint is rotated around the  $y$ -axis, the displacement increment of the node  $i$  in the  $x$  and  $z$  directions is:

$$\left. \begin{aligned} \Delta u &= r_{zi} \sin \theta_y \\ \Delta w &= r_{zi} (1 - \cos \theta_y) \end{aligned} \right\} \quad (4)$$

In the formula,  $r_{zi}$  is the projection distance of  $\rho_i$  on the  $Z$  axis:  $r_{zi} = \rho_i \cos \alpha_i$ .

When the joint is rotated around the  $z$ -axis, the displacement increment of the node  $i$  in the  $x$  and  $y$  directions is:

$$\left. \begin{aligned} \Delta u &= -r_{yi} \sin \theta_z \\ \Delta v &= -r_{yi} (1 - \cos \theta_z) \end{aligned} \right\} \quad (5)$$

In the formula,  $r_{yi}$  is the projection distance of  $\rho_i$  on the  $Y$  axis:  $r_{yi} = \rho_i \sin \alpha_i$ .

According to the formulas (2)~(5), the relationship between the displacement parameters of the beam element nodes and the displacement parameters of the shell element can be obtained as follows:

$$\left. \begin{aligned} u_i &= u + r_{zi} \sin \theta_y - r_{yi} \sin \theta_z \\ v_i &= v - \rho_i [\sin \alpha_i - \sin(\alpha_i - \theta_x)] - r_{xi}(1 - \cos \theta_z) \\ w_i &= w + \rho_i [\cos(\cos \alpha_i - \theta_x) - \cos \alpha_i] + r_{zi}(1 - \cos \theta_y) \end{aligned} \right\} \quad (6)$$

To omit high-order small quantities, Eq. (7) can be simplified as:

$$\left. \begin{aligned} u_i &= u + r_{zi}\theta_y - r_{yi}\theta_z \\ v_i &= v - r_{xi}\theta_x \\ w_i &= w + r_{yi}\theta_x \end{aligned} \right\} \quad (7)$$

Therefore, the constraint equations of the beam element node displacement parameters and the plate-element i-node displacement parameters at the interface are obtained as follows:

$$\left. \begin{aligned} u_i - u - r_{zi}\theta_y + r_{yi}\theta_z &= 0 \\ v_i - v + r_{xi}\theta_x &= 0 \\ w_i - w - r_{yi}\theta_x &= 0 \end{aligned} \right\} \quad (8)$$

$(i = 1, 2 \dots n)$

Formula (8) is the constraint equation of the node displacement parameters at the interface between the beam element and the shell element in the multi-scale model. In this paper, the direct introduction method is adopted. According to the constraint equations, the displacement of the beam element nodes at the interface is used to represent the displacement of the shell element nodes which is introduced into the stiffness matrix and load vector of the shell model. The multi-scale model established is shown in Fig. 7.

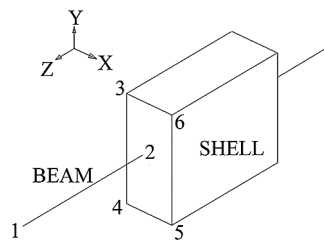


**Figure 6:** The interface between the beam and the shell element

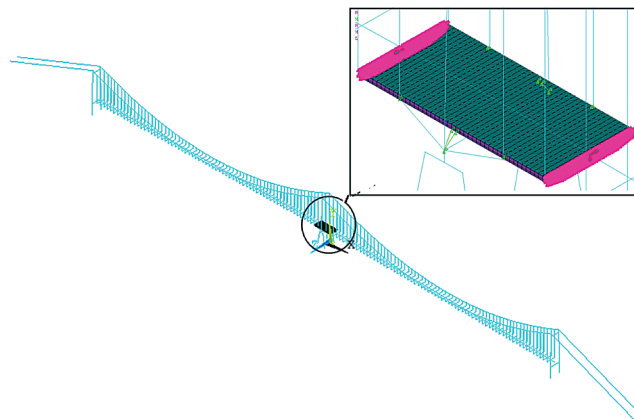


**Figure 7:** The multi-scale model of the Taizhou Yangtze River Bridge

### 3 Analysis of the Most Unfavorable Lane in Steel Box Girder Based on Surveying Vehicle Load

#### 3.1 Fatigue Vehicle Load Model

Considering the actual situation in China, combined with the traffic load survey data of the Jiangyin Yangtze River Bridge, Humen Bridge, Nanjing Second Bridge and Nanjing Third Bridge, the vehicle load model used for the model loading is obtained from the perspective of fatigue. The vehicle load model and the tire grounding diagram are shown in Fig. 8.

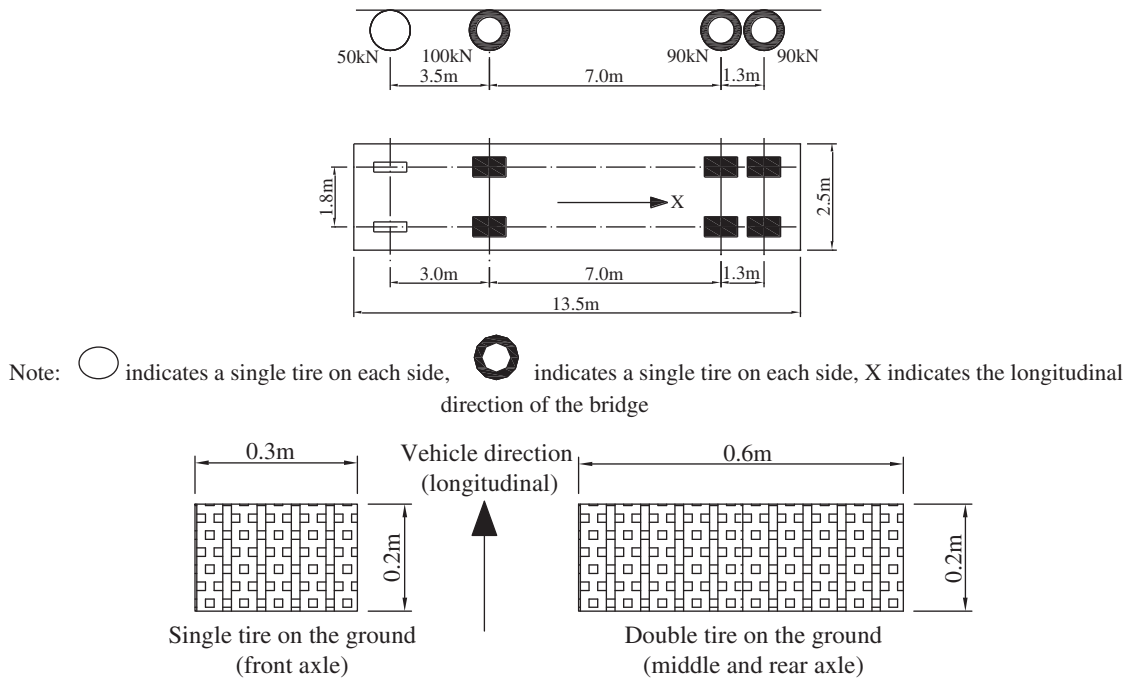


**Figure 8:** The vehicle load model and the tire grounding diagram

#### 3.2 Welded Details and Cross-Sectional Position

In this paper, three welding details are determined according to the lateral position of the Taizhou Yangtze River Bridge wheel load on the lane, as shown in Fig. 9. Two cross sections were selected in the steel box girder segment to analyze the stress characteristics of the six weld details. The Section 1 is located at the position of the first boom on the left side of the middle tower, and the longitudinal bridge coordinate of the section are  $X = -20$  m. The Section 2 is located in the middle of two diaphragms, and its longitudinal bridge coordinates are  $X = -18.4$  m, and the cross-sectional positions are shown in Fig. 10.

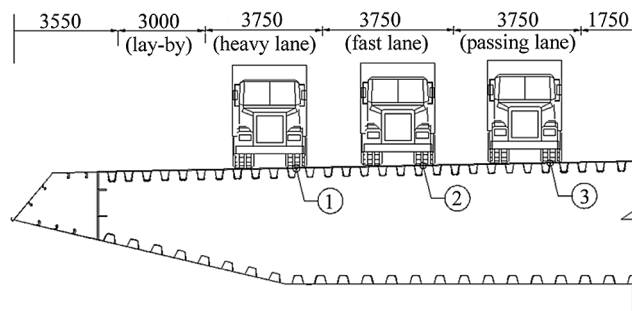


**Figure 9:** Three welded details in one cross section

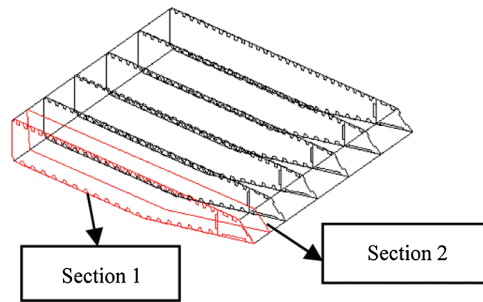


**Figure 10:** Two cross section positions

### 3.3 Loading Mode

In order to obtain the maximum stress response under the wheel load, the loading mode of line load used in this paper (taking the welded detail 1 as an example) is shown in Fig. 11.

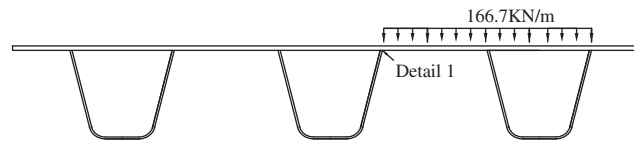


**Figure 11:** The loading mode of welded detail 1

### 3.4 Lane Survey and Selection of Vehicle Loads

The bridge deck Taizhou Yangtze River Bridge is arranged in two-way six lanes. The lane division is shown in Fig. 12. The proportion of traffic flow in each lane during the survey period is shown in Fig. 13. The traffic flow, the mean weight, the standard deviation, and the coefficient of variation of each lane are shown in Tab. 2.

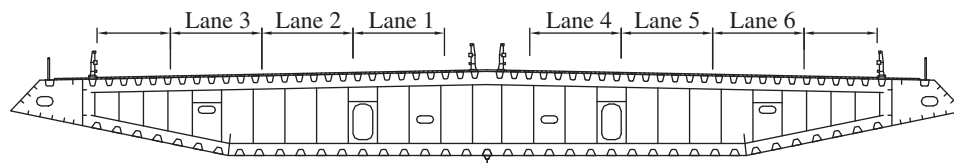


**Figure 12:** The lane division of the Taizhou Yangtze River Bridge

In the fatigue analysis, the vehicle weight average load is used as the fatigue load, and the fatigue load is simplified to the line load applied to each lane of the overall multi-scale model. The concentrated load of vehicles corresponding to the passing lane, fast lane and heavy lane of Taizhou Yangtze River Bridge is 19 kN, 79.9 kN, 132.8 kN, and the length of the lateral wheel landing is 0.6 m. The simplified line loads are 31.7 kN/m, 133.2 kN/m and 221.3 kN/m, respectively. The loading diagram is shown in Fig. 14.

### 3.5 Stress Characteristics Analysis of Welded Details

Since the diaphragm is provided at the cross Section 1, the stress of the welded detail is less than that of the cross Section 2. To save space, this section only analyzes the welded details of the cross Section 2 to determine the most unfavorable lane based on the investigation of the vehicle load. Fig. 15 is the longitudinal and transverse bridge stress nephogram of the steel box girder roof when the details of the Section 2 coincide with the load of the vehicle. It can be seen from the figures that when the load acts on

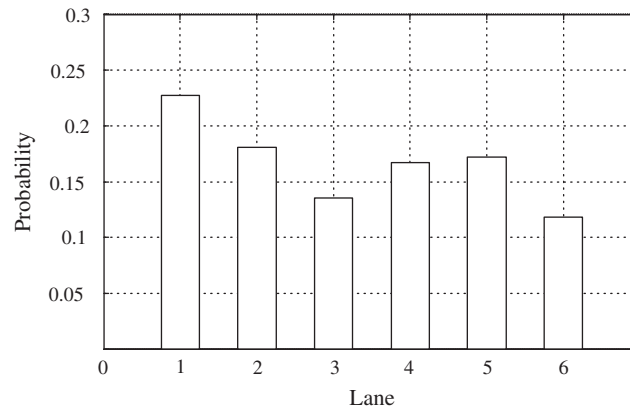


**Figure 13:** The proportion of traffic flow on each lane

**Table 2:** Distribution statistics of vehicles on each lane

Lane	Amount	Proportion (%)	The average of the vehicle weight (t)	The standard deviation of the vehicle weight (t)	Coefficient of variation
Lane 1	1129826	22.73	1.90	2.70	1.42
Lane 2	897085	18.05	7.99	8.37	1.05
Lane 3	672108	13.52	13.28	11.53	0.87
Lane 4	829820	16.70	2.01	3.15	1.57
Lane 5	855156	17.21	7.67	7.96	1.04
Lane 6	586293	11.80	10.06	9.70	0.96

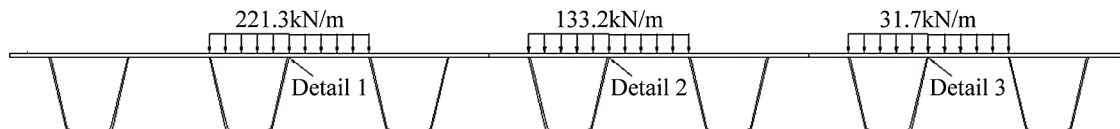
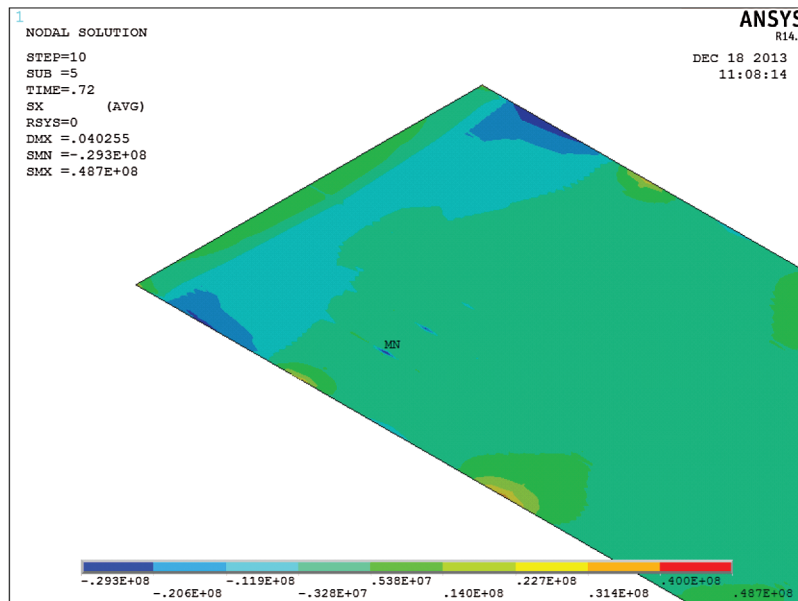


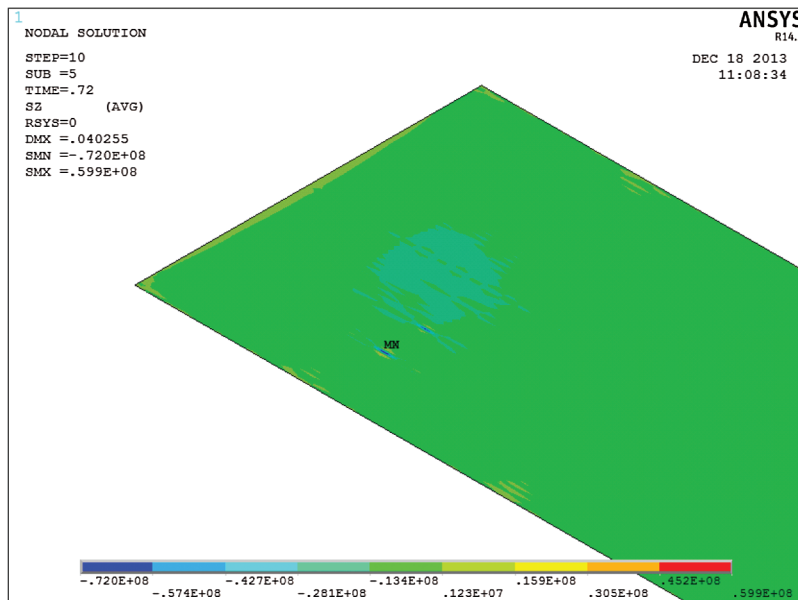
**Figure 14:** The loading diagram of the steel box girder

the Section 2, the stress concentration effect of the bridge deck at the Detail 1 and the Detail 2 is relatively obvious, and the stress concentration effect of the Detail 3 is not obvious, as the load acting on Detail 3 is smaller than the other two loads, so the stress response is not significant.

Fig. 16 is a longitudinal and transverse stress response curve for each weld detail of Section 2, in which the horizontal coordinates represent the load position and the 0 points indicate that the load is acting just at the welded detail. According to the stress time history data obtained using finite element method, the stress amplitude and cumulative fatigue damage of each welded detail at two sections are obtained using the rain flow counting method and the Palmgren-Miner linear damage accumulation theory respectively, as shown in Tab. 3.



(a)



(b)

**Figure 15:** Stress nephogram of bridge deck slab under vehicle load. (a) The longitudinal bridge stress nephogram. (b) The transverse bridge stress nephogram

The following conclusions can be obtained through the analysis of Fig. 16 and Tab. 3:

1. Longitudinal and transverse stress influence lines of each welded detail at the Section 2 under the investigated vehicle load are very short, the length of the influence line is about one and a half diaphragm spacing (4.8 m). The transverse stress is greater than the longitudinal stress, the maximum transverse stress is 74.5 Mpa and the maximum longitudinal stress is 29.9 MPa, both located at the welded detail 3. At the same time, the transverse stress amplitude is larger than the longitudinal stress amplitude, and the transverse fatigue damage of detail 1 is the largest, and the value is  $8.94 \times 10^{-7}$ .

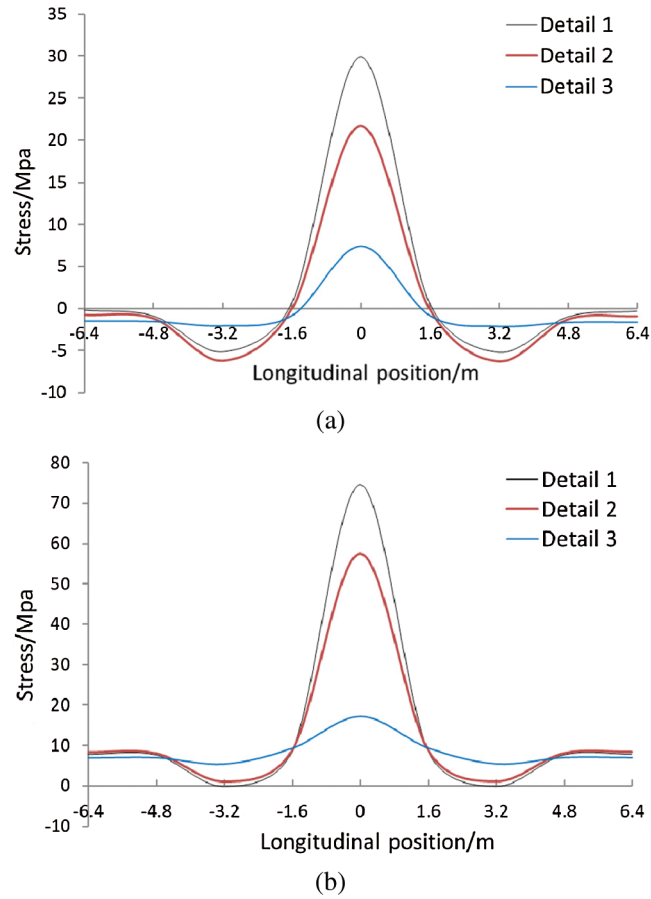


**Figure 16:** Stress response of each welded detail at the Section 2. (a) Longitudinal stress. (b) Transverse stress

**Table 3:** Stress amplitude and fatigue damage of each detail at Section 2

Working condition	Longitudinal bridge direction			Transverse bridge direction		
	Detail 1	Detail 2	Detail 3	Detail 1	Detail 2	Detail 3
Stress amplitude (MPa)	4.92	5.38	0.56	7.94	7.28	1.54
	35.08	27.90	9.53	74.51	56.41	11.64
Fatigue damage ( $\times 10^{-10}$ )	933.3	322.0	1.5	8942.7	3880.7	4.1
Traffic flow	672108	897085	1129826	672108	897085	1129826
Accumulated Fatigue damage	0.062	0.028	0.0002	0.60	0.35	0.0005

- Welded detail 1 has the highest stress response, so the fatigue damage is also the largest, the Detail 2 takes second place, and the Detail 3 is the smallest. The load acting on the heavy lane is 132.8 KN, which is 1.67 times that acting on the fast lane (79.9 KN) and 6.99 times that acting on the passing lane (19 KN). Although the support conditions of the steel box girder and the special construction of the heavy lane will lead to the reduction of the stress response of Detail 1, the stress response of the

heavy lane is still the largest due to the large difference in load, and the fatigue damage is also the most obvious.

3. According to the traffic flow survey, the traffic flow on the heavy lane, fast lane and passing lane is 672108, 897085, 1129826 respectively. The most vehicles are on the passing lane, the fast lane is the second, and the heavy lane is the least. Through the traffic flow and the fatigue damage under the action of single vehicle, the cumulative fatigue damage of each detail in the same time period can be obtained. Detail 1 has the largest cumulative fatigue damage with a value of 0.6. Since the vehicle load is simplified to a single wheel load, the calculated stress is rather large, and the cumulative fatigue damage is also rather large. This section examines the relative fatigue damage of the three details, so the above deviations can be negligible.

It can be seen from the above analysis that the stress response of Detail 1 is the largest based on the investigated vehicle load. When a wheel load of 132.8 KN is applied, the fatigue damage is  $8.94 \times 10^{-7}$ , which means that when 1.12 million identical wheels pass, the cumulative fatigue damage of this detail is 1, and fatigue damage may occur. Through the traffic flow statistics, the cumulative fatigue damage of each detail in the same time period can also be obtained. The cumulative fatigue damage of Detail 1 is the largest, and it will be destroyed before the other two details. The investigated vehicle load reflects the real situation of the traffic flow on the bridge, so the stress response under the investigated vehicle load can reflect the actual stress of the steel box girder. Detail 1 is located in the heavy lane and is the most unfavorable lane for fatigue analysis.

#### 4 Welded Detail Selection and Model Loading Result Analysis

##### 4.1 Welded Detail Selection

The orthotropic steel bridge deck has a relatively large ultimate bearing capacity under uniform load, but due to the thin bridge deck, under the concentrated load of the wheel, a relatively large local deformation will occur, and its vertical deformation causes the relative angle with the longitudinal ribs to produce a relatively large stress, and the weld at the connecting part is subjected to the bending tensile stress, which is prone to fatigue cracking. This type of weld is the most common in steel box girder and directly bears the load of the wheel, so this position is the welded detail to be considered in this paper.

The longitudinal rib can be regarded as a continuous beam elastically supported on the diaphragm. The bridge deck structure is composed of bridge deck, transverse ribs and the longitudinal ribs. The longitudinal rib mainly plays the role of longitudinal beam in the bridge deck system, so the bottom of it is subjected to bending tensile stress and the effect is relatively obvious. The connection of the longitudinal ribs is docked by the inlay section, and is in the position of the overhead welding when the field welding is performed. The working conditions are bad and the welding quality is difficult to ensure, so this position is also the welding detail to be investigated in this paper. The two specific positions of two welded details correspond to the Welds 1 and 2 of Fig. 17, respectively.

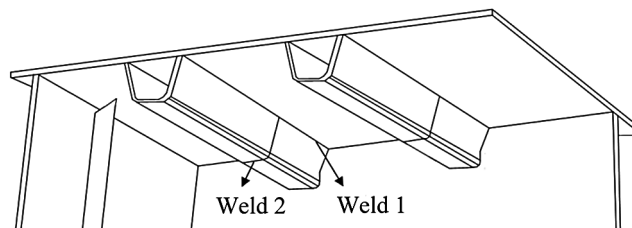


**Figure 17:** The positions of the two welded details

#### 4.2 Orthotropic Steel Bridge Deck Model and Loading Condition

According to the structural parameters of the steel box girder in Section 2.1, a refined model of the orthotropic steel bridge deck is established (the thickness of the roof is 14 mm, the thickness of the longitudinal rib is 6 mm, and the thickness of the diaphragm is 10 mm), as shown in Fig. 17. The roof, longitudinal ribs and diaphragms of the model were simulated by using shell63. The model mesh is densely divided, and the size of the roof mesh is 50 mm × 100 mm, which can facilitate the application of wheel load and accurately output element stress.

Considering the range of load stress, the vehicle load model in Section 3.1 is used for loading simulation. For the convenience of loading, the wheel load is equivalent to the surface load, and the vehicle surface pressure is 0.417 MPa. The wheel load is moved longitudinally from the first diaphragm position to the fifth diaphragm position, every time moving 200 mm for a total of 80 load steps. The loading diagram is shown in Fig. 18.

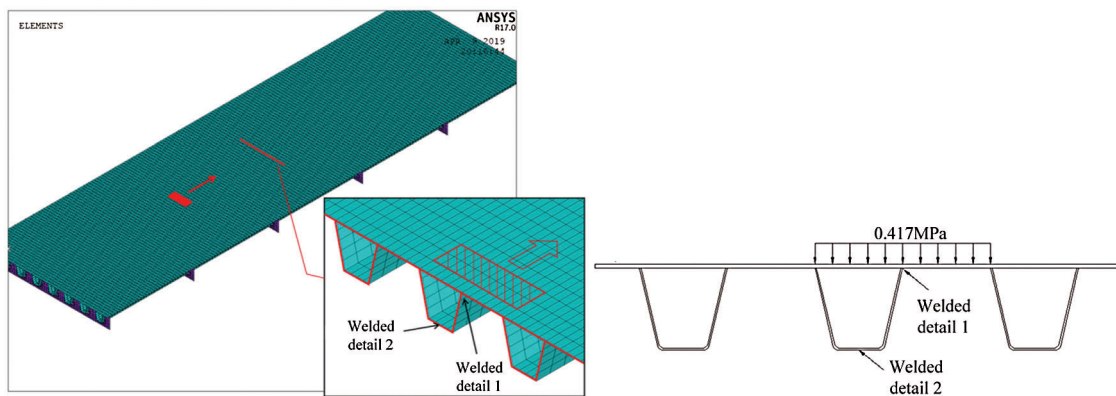


**Figure 18:** The diagram of the orthotropic steel bridge deck model loading

#### 4.3 Stress Characteristics Analysis of Welded Details under Wheel Load

Welded detail 1 is a longitudinal bridge weld, and the transverse bridge stress is taken as the reference stress. Weld 2 is the transverse bridge weld, and the longitudinal bridge stress is extracted as the reference stress. The positions of the two welds are shown in Fig. 17. Fig. 19 shows the stress response curves of the upper surface (TOP), the middle surface (MID) and the lower surface (BOT) of Weld 1 and welded detail 2 under wheel load, respectively, to analyze the stress characteristics of the welded detail. The position of three kinds of surface are shown in shell63 unit in Fig. 5. The longitudinal coordinates represent the amount of the stress, and the horizontal coordinates represent the load position.

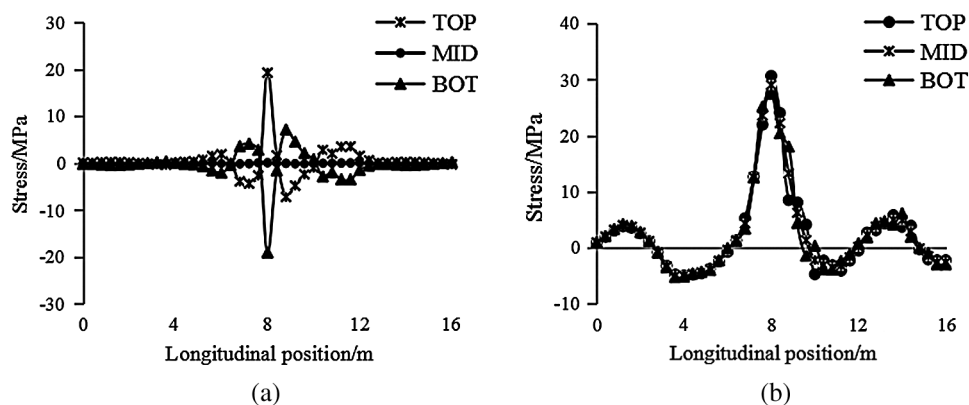


**Figure 19:** The stress curves of the welded detail under the wheel load. (a) The stress curve of the welded detail 1. (b) The stress curve of the welded detail 2

The following conclusions can be obtained by analyzing Fig. 19:

1. The longitudinal bridge stress influence lines of welded details 1 and 2 are relatively short. When the load acts directly on the weld, the stress response is the largest, showing a very obvious local characteristic.
2. The stresses of the upper and lower surfaces are positive and negative respectively, and the absolute values are substantially equal, and the mid-surface stress is small. This shows that when the wheel load is applied, the upper surface is pulled and the lower surface is pressed. The weld 1 is basically in a purely bending state, and the influence of the membrane stress can be ignored. Therefore, transverse bending stress is used as the referenced fatigue stress for welded details 1.
3. For welded detail 2, the stress values of the upper, middle and lower surfaces are substantially equal. This indicates that under the wheel load, the bottom of the longitudinal rib is pulled, and the welded detail 2 is basically only affected by the in-plane load, and the longitudinal membrane stress can be used as the referenced fatigue stress of the Weld 2.

## 5 The Real Bridge Test Study on the Welded Detail

The finite element method has clear concepts and it is a very effective method for fatigue analysis of steel box girder. At the same time, the real bridge test is also a very important method. This method can more accurately reflect the true force of the bridge. Based on the load test of Taizhou Yangtze River Bridge, the stress, distribution and law of key welded details of orthotropic steel bridge deck under the action of vehicle are studied in this paper.

### 5.1 Measuring Point Arrangement and Loading Conditions

The statistics of the real bridge show that the fatigue effect of the steel box girder at the position of the first boom on the left and right sides of the middle tower is the most obvious, which is the key part of fatigue analysis. Therefore, the test is carried out on the steel box girder at the first boom position on the left side of the middle tower. The measuring points are arranged laterally at the longitudinal ribs of Nos. 13-18. The position consists of two types of bridge decks (the roof is 14 mm thick and the longitudinal rib is 6 mm thick at the position of Nos. 13-15 longitudinal ribs; the roof is 16 mm thick and the longitudinal rib is 8 mm thick at the position of Nos. 16-17 longitudinal ribs). The test position of the steel box girder is shown in Fig. 20.

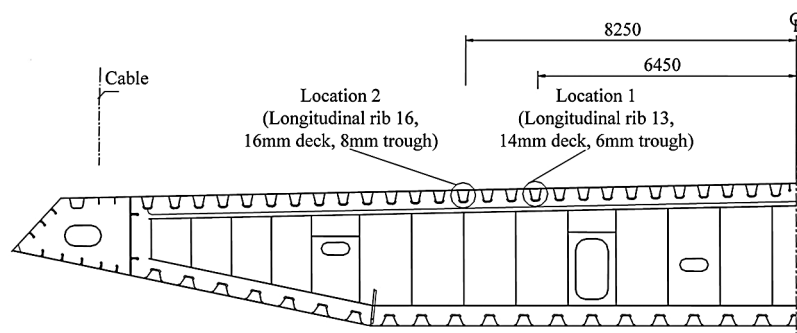


**Figure 20:** Test location diagram

The measuring points are symmetrically arranged at the positions of the 14 mm and 16 mm thick deck plate. If there is no diaphragm at the position, the roof is provided with one-way and two-way strain gauges in order to monitor the longitudinal and transverse stress of the rib-to-deck welded connection, and the rib-to-rib welded connection is provided with one-way strain gauges in the longitudinal bridge direction. If there is

diaphragm at the position, due to the complex stress distribution of each welded detail at the diaphragm, the strain rosette is arranged on the diaphragm, and the roof is arranged with one-way and two-way strain gauges. The measuring point arrangement is shown in Fig. 21.

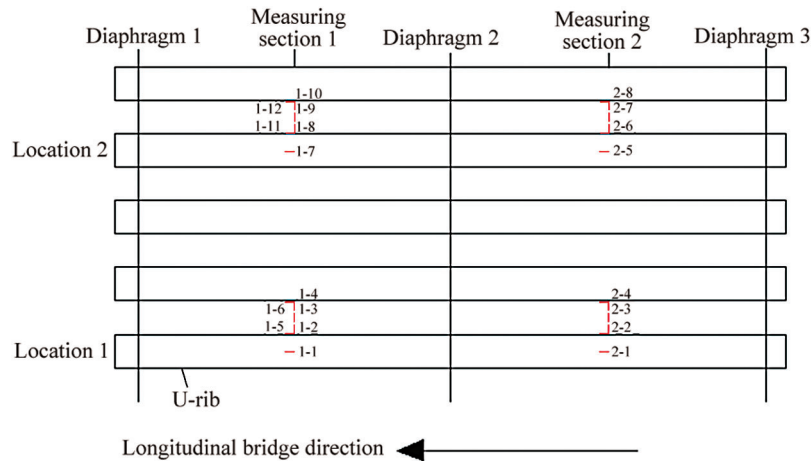


**Figure 21:** Diagram of the measuring point arrangement

Data were collected on site using DH 3817 and TEST 3827 dynamic and static signal test instruments. There are 8 test channels for each instrument, and each instrument is connected in series. The strain gauge connection mode is 1/4 bridge, and make temperature compensation. The sampling frequency is 100 Hz. Fig. 22 is a field photograph.



**Figure 22:** Field measured photos

The test loading vehicle adopts a 3-axle truck with a total weight of 30t. The front axle has a weight of 60 kN, the middle axle and rear axle are both 120 kN. The distance between the middle and front axles is 3500 mm and the distance between the middle and rear axles is 1350 mm, and the wheelbase is 1800 mm. The vehicle model diagram is shown in Fig. 23.

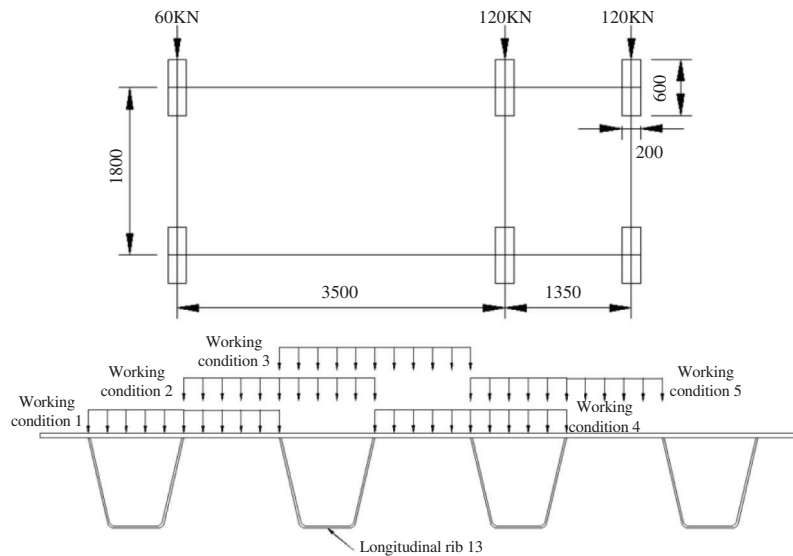


**Figure 23:** Vehicle model and working conditions diagram

This test is divided into single-vehicle test and fleet test. In the single-vehicle test, a fatigue vehicle is used to pass through the bridge in the longitudinal direction and is divided into five working conditions. The lateral position of the wheel in each working condition differs by 300 mm. The lateral arrangement of the wheel is shown in Fig. 23 (take the longitudinal rib No. 13 as an example). In the fleet test, 12 identical fatigue vehicles were used to pass through the bridge one by one in the longitudinal direction, and the longitudinal spacing of two adjacent vehicles is 20 m. The speed of the vehicle is 40 km/h, and the lateral position of the wheel is the same as that of the single-vehicle test under the working condition 3.

## 5.2 Stress Analysis of Welded Detail in Single-Vehicle Test

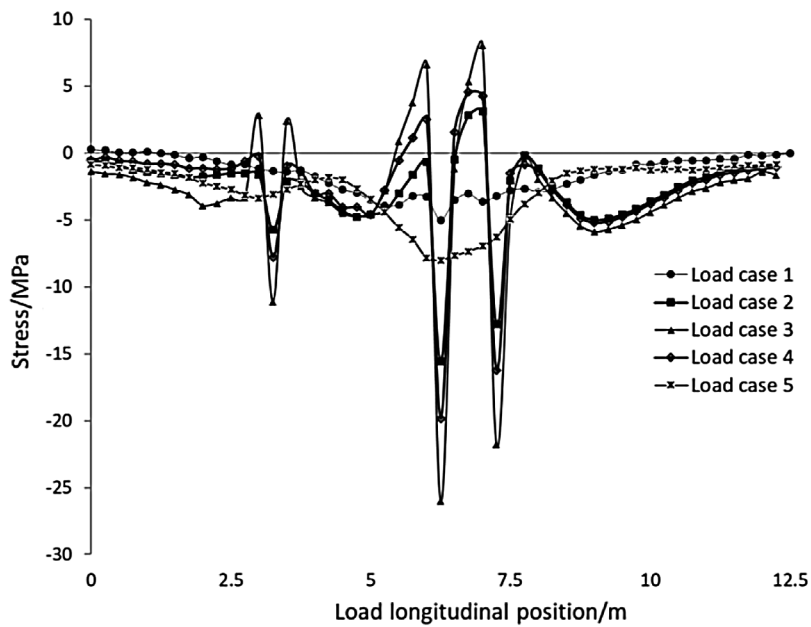
### 5.2.1 Welded Detail 1

There are many measuring points in this test. The same test item will have different sections for comparison, and the same law is obtained in the analysis. In order to save space, this paper lists several typical measuring points. The typical stress distribution of the measured points is shown in Fig. 24.

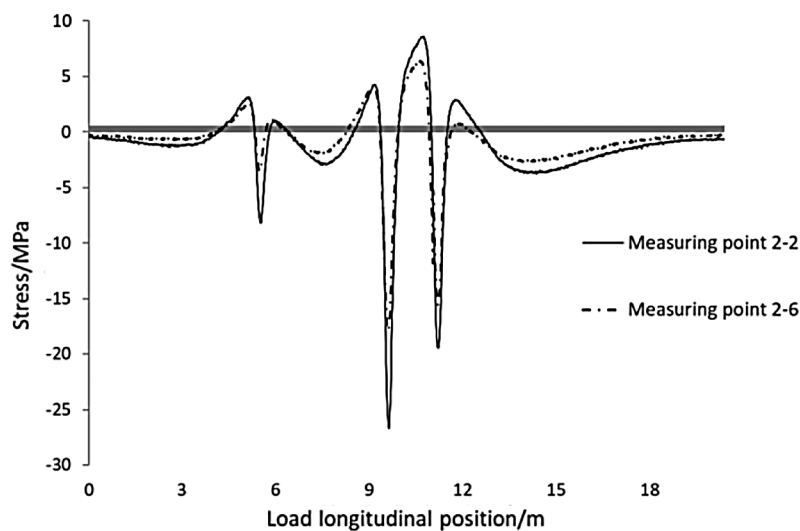
Fig. 24a shows the stress curves of measuring point 2-2 under different working conditions, in which the horizontal coordinates represent the longitudinal action position of the load and the longitudinal coordinates represent the stress amount. The following conclusions can be obtained from the Fig. 24a:

1. When under working conditions 2, 3 and 4, the measuring point stress curve has three troughs, the first trough is about 3.5 m away from the second trough, and the second trough is about 1.5 m away from the third trough. This is consistent with the wheelbase of the vehicle. Therefore, it can be inferred that the three troughs are caused by the direct action of the wheel load, and the lower surface of the roof is pressed under the wheel load.
2. Under working condition 3, the wheel load center coincides with the measuring point 2-2, and the stress response is the most obvious; under working conditions 2 and 4, the wheel load center is

closer to the measuring point, and the stress response trend is the same as that of working condition 3, but the stress is smaller; under working conditions 1 and 5, the wheel load center is far from the measuring point, the stress response is small, and the trend is not obvious. The above analysis shows that the stress response of the roof has strong local characteristics under the wheel load, and the influence line of the lateral stress on the roof is relatively short, which is greatly affected by the longitudinal ribs.



(a)



(b)

**Figure 24:** Stress curve of two measuring points under different working conditions. (a) Point 2-2 in different load cases. (b) Points 2-2 and 2-6 in load case 3

The test site of this test contains two positions, and the roof and the longitudinal rib at the position are locally thickened. It can be seen from the Fig. 24(b) that the stress response trends of the two measuring points are the same, but the stress values of measuring point 2-6 are smaller. Under the action of the middle axle load, the stress value of the point 2-6 is  $-17.2$  MPa, which is 35% lower than the stress value of point 2-2. Therefore, it can be inferred that thickened roof and longitudinal rib can improve the mechanical performance of this welded detail.

### 5.2.2 Welded Detail 2

Fig. 25a shows the stress curve of measuring point 2-1 under different working conditions, and Fig. 25b shows the stress curve of measuring points 2-1 and 2-5 under working condition 3. The horizontal coordinates represent the longitudinal action position of the load and the longitudinal coordinates represent the stress amount. It is found through analysis that this welded detail has the same regularity as the welded detail 1:

1. The stress response of the longitudinal rib has strong local characteristics under the wheel load, and the influence line of the lateral stress on the longitudinal rib is relatively short, which is greatly affected by the longitudinal ribs.
2. Thickened deck plate and longitudinal rib can reduce the stress response of the longitudinal rib and improve the mechanical performance of this welded detail.

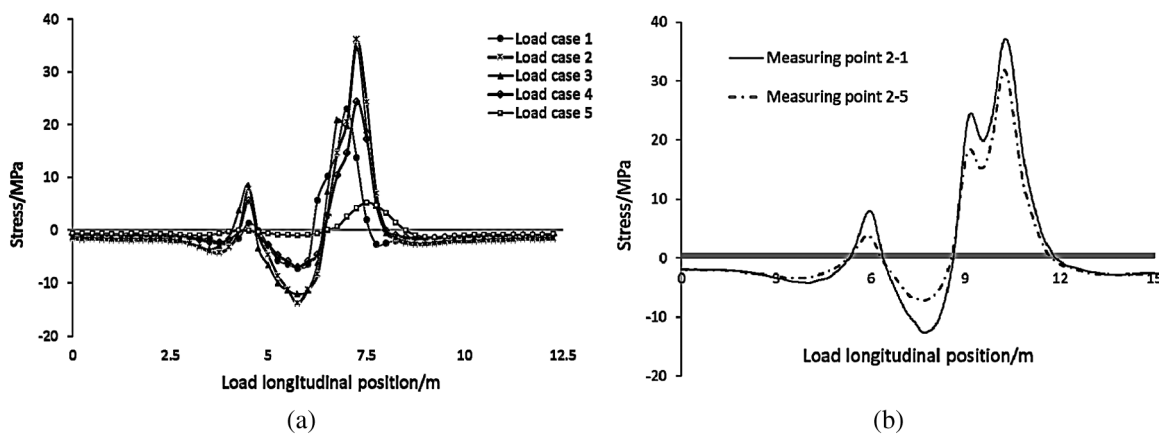


**Figure 25:** Stress curve of two measuring points under different working conditions. (a) Point 2-1 in different load cases. (b) Points 2-1 and 2-5 in load case 3

### 5.3 Comparative Analysis of Single-Vehicle Test and Finite Element Calculation

In addition to the real bridge test, the finite element calculation is carried out in this paper, and the analysis results of the real bridge test are compared and verified. The study in Section 3 above shows that the fatigue effect of heavy lanes is the most obvious during the bridge operation, which is the most unfavorable position for fatigue analysis. Therefore, this paper only analyzes the two welded details (shown in the Fig. 17) at the position of the heavy lane.

In order to be consistent with the actual force of the bridge, the multi-scale model of the Taizhou Yangtze River Bridge was used to analyze the stress of the bridge deck welding details at the position of the heavy lane. The steel box girder meshing of the multi-scale model established in Section 2.2 is rough, and it is not convenient to apply the wheel load. It is necessary to encrypt the steel box girder mesh. However, the whole model encryption will make the amount of the element and node very large, the calculation efficiency is low, and the stress response of the bridge deck has a strong local characteristic when the wheel load acts, and the

whole model encryption is not necessary. Therefore, the bridge deck of the heavy lane position is partially refined, and the encrypted roof grid size is  $50 \text{ mm} \times 100 \text{ mm}$ , which is convenient for the application of wheel load, and the extracted stress is more accurate. The encrypted multi-scale model is shown in Fig. 26.

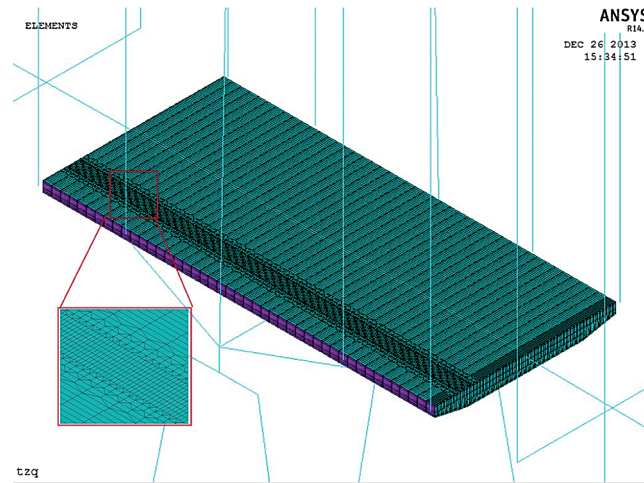


**Figure 26:** Steel box girder segment model with refined heavy lane

The encrypted steel box girder segment model is effectively connected with the spine beam model by the mangle unit method, and the established multi-scale model is shown in Fig. 27.

The single-side wheel load of three-axle truck in the load test is applied to the model, and the stress response curve of the bridge deck welded detail at the position of the heavy lane is obtained as shown in Fig. 28. It can be found through comparing Fig. 28 with Figs. 24 and 25 that: The trend of the stress response curve obtained by finite element calculation is consistent with the real bridge test. Under the direct action of the wheel load, the stress response curve of the welded detail has a sudden change, and has obvious local characteristics. The stress value obtained by the finite element calculation is larger than that obtained by the real bridge test. This is because the deck is covered with a pavement layer, the wheel load will spread to the deck along the thickness of the pavement layer at an angle of  $45^\circ$ , the load acting area is increased, the surface load is relatively reduced, and the stress concentration effect is also reduced, so the measured value is smaller than the calculated value. By comparison, it can be inferred that the above-mentioned locally refined multi-scale model can be used to calculate the stress response of two welded details relatively accurately.

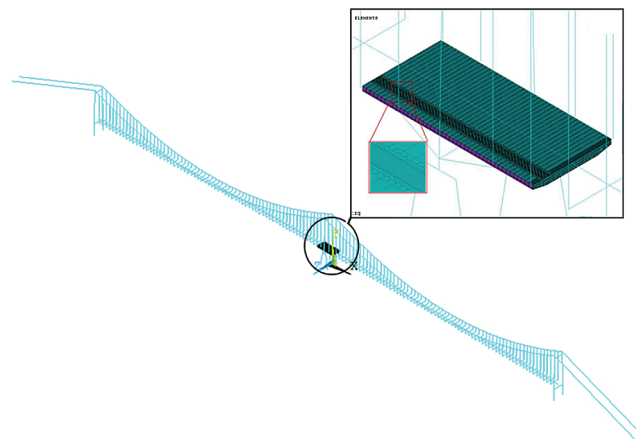


**Figure 27:** The encrypted multi-scale model of the Taizhou Yangtze River Bridge

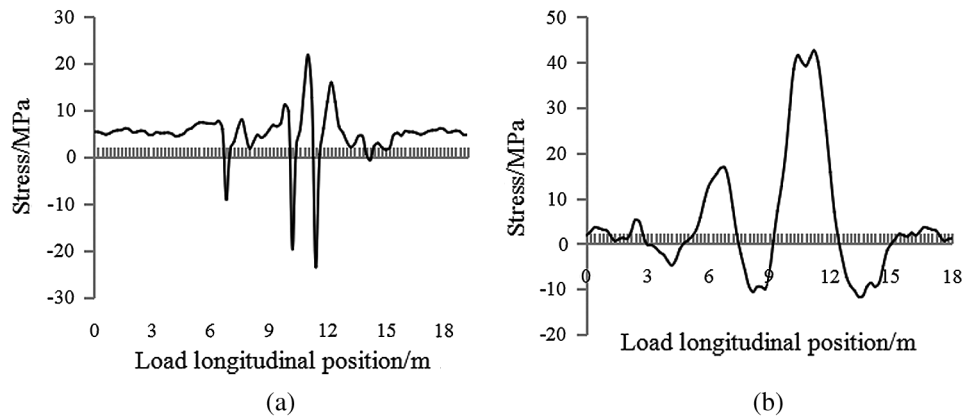


**Figure 28:** Stress curve of two welded details obtained by finite element method. (a) Stress curve of welded detail 1. (b) Stress curve of welded detail 2

#### 5.4 Fatigue Damage Analysis of Welded Detail under Fleet Test

In the fleet test, twelve identical fatigue vehicles were used to pass through the bridge in the longitudinal direction. The lateral position of the wheel is shown in working condition 3 in Fig. 23. Fig. 29 shows the stress time history of each welded detail under the load of the fleet. As can be seen from the Fig. 29, when each vehicle passes, the stress of each detail will mutate. There are 12 vehicles in the fleet test, so there are twelve mutations in the stress time history curve. There will be a large error in the lateral position of the vehicle during the driving process, coupled with the local characteristics of the stress under wheel load, so the stress value at each mutation is different. Since the distance between the track and the two test positions are fixed, the lateral position deviation of the wheel is the same for each welded detail, so this error can be ignored in the study of the cumulative fatigue damage at each welded detail. The roof and longitudinal ribs of the heavy lane are locally thickened, which improves the mechanical performance of the bridge deck. Therefore, the stress of the two welded details on Location 2 is less than the stress of the corresponding welded detail on Location 1 as shown in Fig. 20.

For the stress time history data of the 4 welded details, the rain flow counting method can be used to obtain the stress amplitude for each detail, as shown in Tab. 4 and Fig. 30. It can be seen that the stress amplitude less than 5 MPa occupies the majority of the stress cycle, which is caused by the vibration of the bridge due to the joint action of environmental factors and vehicle loads. The maximum stress amplitude of the four welded details is greater than the fatigue limit (35 MPa), but the amplitude of stress cycle below the fatigue limit is the majority. Therefore, the combination of high amplitude stress cycle and low amplitude stress cycle should be considered in the fatigue life assessment.

The fatigue problem for steel bridge structure has the characteristics of variable amplitude and long life. It is necessary to study the fatigue performance of steel bridge under variable amplitude fatigue load, so the fatigue damage accumulation theory is introduced. The fatigue damage accumulation theory holds that the total fatigue damage is equal to the sum of the damage under various fatigue loads. At present, the most widely used is the Palmgren-Miner linear damage accumulation theory, which holds that the whole fatigue damage is a linear superposition of fatigue damage caused by each variable amplitude stress cycle. According to the Palmgren-Miner linear damage accumulation theory, the fatigue damage of the detail under the variable amplitude load is:

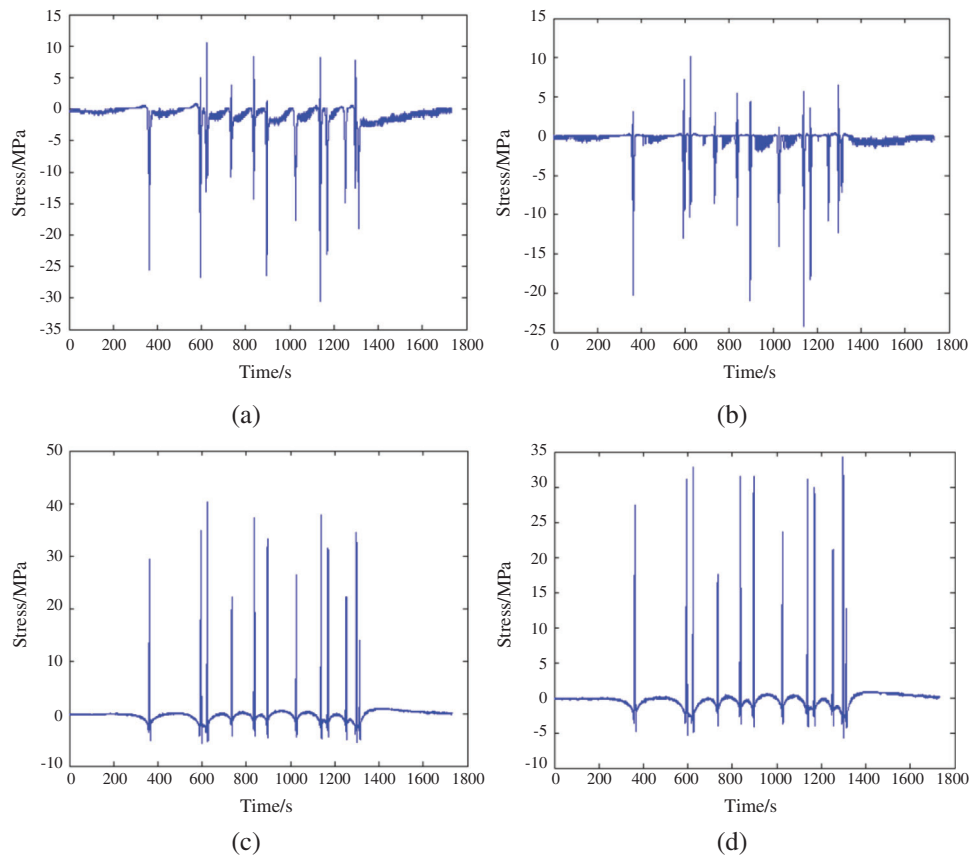


**Figure 29:** Stress response curve of two welded details at two locations. (a) Welded detail 1 on Location 1. (b) Welded detail 1 on Location 2. (c) Welded detail 2 on Location 1. (d) Welded detail 2 on Location 2

**Table 4:** Stress amplitude spectrum for each welded detail

Number of loops	Stress amplitude (MPa)										
	0-5	5-10	10-15	15-20	20-25	25-30	30-35	35-40	40-45	45-50	
Welded detail	1-1	443	4	6	3	4	4	2	2	1	0
	1-2	526	10	7	4	3	1	3	0	0	0
	2-1	618	5	0	3	1	3	0	3	3	1
	2-2	578	3	1	1	2	1	5	5	1	0

$$D = \sum_{S_i \geq S_0} \frac{n_i S_i^3}{K_2} + \sum_{S_j < S_0} \frac{n_j S_j^5}{K_2 S_0^2} \quad (9)$$

In the formula,  $n_i$  and  $n_j$  represent the number of stress cycles equal to or greater than  $S_0$  and less than  $S_0$ , respectively.

The fatigue damage increment of each weld detail in the fleet test can be obtained according to formula (9), as shown in Tab. 5. It can be seen from the table that: For the welded detail 1, the fatigue damage

increment of Location 1 is 2.6 times that of the Location 2; for the welded detail 2, the fatigue damage increment of Location 1 is 1.5 times that of the Location 2. It can be seen that the thickened roof and longitudinal ribs can reduce the fatigue damage of the welded details and improve the fatigue performance of the bridge deck. At the same time, the fatigue damage of welded detail 2 is greater than that of welded detail 1, so the fatigue performance of rib-to-rib connection weld should be paid more attention when the bridge design and maintenance are carried out.

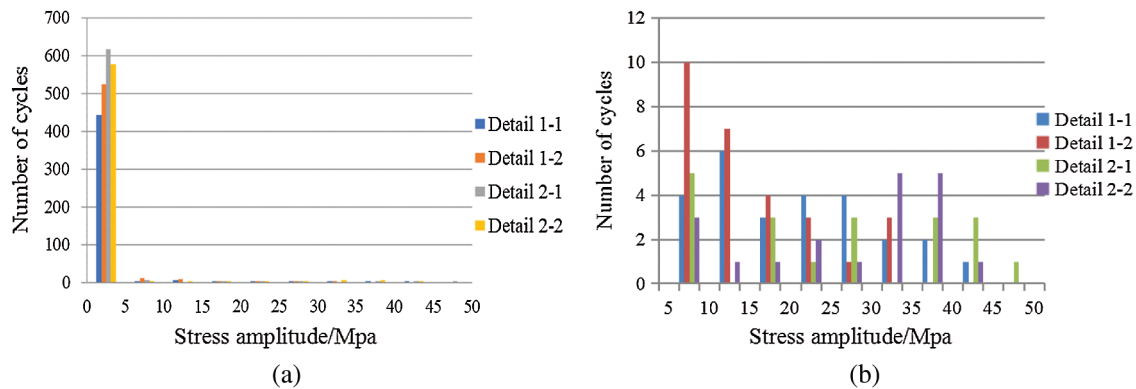


**Figure 30:** Stress amplitude histogram for each welded detail. (a) Stress amplitude histogram. (b) Stress amplitude > 5 MPa

**Table 5:** Fatigue damage increment of each welded detail

Welded detail	1-1	1-2	2-1	2-2
Fatigue damage increment ( $\times 10^{-7}$ )	6.66	2.56	12.00	7.89

## 6 Conclusion

1. Through the comparative analysis of experimental results and multi-scale model results, it can be seen that the multi-scale model in this paper is reasonable and accurate.
2. The cumulative fatigue damage of the bridge deck at the heavy lane position is greater than that of the fast lane and passing lane during the same time, so the heavy lane is the most unfavorable lane for fatigue analysis.
3. The upper surface of orthotropic steel bridge deck is pulled and the lower surface is pressed, and the welded detail 1 is basically in a purely bending state, and the influence of the membrane stress can be ignored, therefore, transverse bending stress is used as the referenced fatigue stress of welded detail 1; The bottom of the longitudinal rib is pulled, and the welded detail 2 is basically only affected by the in-plane load, and the longitudinal membrane stress can be used as the referenced fatigue stress of the welded detail 2.
4. The stress response of two welded details has obvious local characteristics, the influence line of transverse stress is short, and the length of influence line is greatly affected by longitudinal ribs. The thickened roof and longitudinal ribs of the heavy lane can reduce the stress response of the two welded details and improve the fatigue performance of the heavy lane.
5. For the two welded details, the fatigue damage increment of the ordinary lane is greater than the heavy lane. The thickened roof and longitudinal ribs at the position of the heavy lane still cannot balance the fatigue damage caused by the heavy truck. Therefore, it is necessary to strictly control the fatigue effect of overloaded vehicles on steel box girders.

**Funding Statement:** This research has been supported by the National Natural Science Foundation of China (Grant No. 51778135), the National Key R&D Program Foundation of China (Grant No. 2017YFC0806001), the Natural Science Foundation of Jiangsu Province, China (Grant No. BK20160207), and Aeronautical Science Foundation of China (Grant No. 20130969010), the Fundamental Research Funds for the Central Universities and Postgraduate Research & Practice Innovation Program of Jiangsu Province, China (Grant Nos. KYCX18\_0113 and KYLX16\_0253).

**Conflicts of Interest:** The authors declare that they have no conflicts of interest to report regarding the present study.

## References

1. Zhu, A., Li, M., Tian, Y., Xiao, H., He, D. et al. (2017). Fatigue test on full-scale orthotropic steel bridge deck with inner diaphragm. *Steel Construction*, 32(217), 45–50.
2. Kainuma, S., Yang, M., Jeong, Y. S., Inokuchi, S., Kawabata, A. et al. (2016). Experiment on fatigue behavior of rib-to-deck weld root in orthotropic steel decks. *Journal of Constructional Steel Research*, 119, 113–122. DOI 10.1016/j.jcsr.2015.11.014.
3. Zhang, Q. H., Cui, C., Bu, Y. Z., Liu, Y. M., Ye, H. W. (2015). Fatigue tests and fatigue assessment approaches for rib-to-diaphragm in steel orthotropic decks. *Journal of Constructional Steel Research*, 114, 110–118. DOI 10.1016/j.jcsr.2015.07.014.
4. Wolchuk, R. (1992). Lessons from weld cracks in orthotropic decks on three European bridges. *Journal of Structural Engineering*, 116(1), 75–84. DOI 10.1061/(ASCE)0733-9445(1990)116:1(75).
5. Tsakopoulos, P. A., Fisher, J. W. (2003). Full-scale fatigue tests of steel orthotropic decks for the Williamsburg Bridge. *Journal of Bridge Engineering*, 8(5), 323–333. DOI 10.1061/(ASCE)1084-0702(2003)8:5(323).
6. Wang, C. S., Fu, B. N., Zhang, Q. (2013). Fatigue test on full-scale orthotropic steel bridge deck. *China Journal of Highway and Transport*, 26(2), 69–76.
7. Zhang, Q. H., Cui, C., Bu, Y. Z. (2014). Study on fatigue features of orthotropic decks in steel box girder of Hong Kong-Zhuhai-Macao Bridge. *China Civil Engineering Journal*, 47(9), 110–119.
8. Zeng, Z. B. (2011). Classification and reasons of typical fatigue cracks in orthotropic steel deck. *Steel Construction*, 26(2), 9–15.
9. Cui, C., Liu, Y. M., Liao, G. X. (2015). Fatigue evaluation approach of weld joints on steel orthotropic bridge deck. *Journal of Southwest Jiaotong University*, 50(6), 1011–1017.
10. Gu, P., Zhou, C. (2012). Estimation of fatigue life of typical fatigue cracks of orthotropic steel decks of railway bridges. *Journal of the China Railway Society*, 34(1), 97–102.
11. Zhang, Q. H., Bu, Y. Z., Qiao, L. I. (2017). Review on fatigue problems of orthotropic steel bridge deck. *China Journal of Highway & Transport*, 30(3), 14–30, 39.
12. Connor, R., Fisher, J., Gatti, W., Gopalaratnam, V., Kozy, B. et al. (2012). Manual for design, construction, and maintenance of orthotropic steel deck bridges. *Integral Leadership Review*, 2012, 1–291.
13. Wang, G., Ding, Y., Song, Y., Wei, Z. (2016). Influence of temperature action on the fatigue effect of steel deck with pavement. *Engineering Mechanics*, 33(5), 115–123.
14. Heng, J., Zheng, K., Gou, C., Zhang, Y., Bao, Y. (2017). Fatigue performance of rib-to-deck joints in orthotropic steel decks with thickened edge U-ribs. *Journal of Bridge Engineering*, 22(9), 04017059. DOI 10.1061/(ASCE)BE.1943-5592.0001095.
15. Fu, Z., Ji, B., Zhang, C., Wang, Q. (2017). Fatigue performance of roof and u-rib weld of orthotropic steel bridge deck with different penetration rates. *Journal of Bridge Engineering*, 22(6), 04017016. DOI 10.1061/(ASCE)BE.1943-5592.0001036.
16. Lu, N. W., Liu, Y., Deng, Y. (2019). Fatigue reliability evaluation of orthotropic steel bridge decks based on site-specific weigh-in-motion measurements. *International Journal of Steel Structures*, 19(1), 181–192. DOI 10.1007/s13296-018-0109-8.

17. Liu, Y. M., Zhang, Q. H., Zhang, P., Cui, C., Bu, Y. Z. (2016). Study on fatigue life of U-rib butt weld in orthotropic steel bridge deck of Hong Kong-Zhuhai-Macao bridge. *China Journal of Highway & Transport*, 29(12), 25–33.
18. Wu, C., Yuan, Y., Jiang, X. (2016). Fatigue behavior assessment method of the orthotropic steel deck for a self-anchored suspension railway bridge. *Procedia Engineering*, 161, 91–96. DOI 10.1016/j.proeng.2016.08.503.
19. Tang, L., Huang, L., Liu, G., Wang, C., Fu, B. (2014). Fatigue experimental study of a full-scale steel orthotropic deck model. *China Civil Engineering Journal*, 47(3), 112–122.
20. Fu, Z., Ji, B., Zhang, C., Li, D. (2018). Experimental study on the fatigue performance of roof and U-rib welds of orthotropic steel bridge decks. *KSCE Journal of Civil Engineering*, 22(1), 270–278. DOI 10.1007/s12205-017-1725-0.
21. Yang, M. Y., Kainuma, S., Jeong, Y. S. (2018). Structural behavior of orthotropic steel decks with artificial cracks in longitudinal ribs. *Journal of Constructional Steel Research*, 141, 132–144. DOI 10.1016/j.jcsr.2017.11.007.
22. Cheng, B., Ye, X. H., Cao, X. G., Mbako, D. D., Cao, Y. S. (2017). Experimental study on fatigue failure of rib-to-deck welded connections in orthotropic steel bridge decks. *International Journal of Fatigue*, 103, 157–167. DOI 10.1016/j.ijfatigue.2017.05.021.
23. Deng, Y., Li, A., Feng, D. M. (2018). Fatigue reliability assessment for orthotropic steel decks based on longterm strain monitoring. *Sensors*, 18(1), 181. DOI 10.3390/s18010181.
24. Zhu, J. S., Guo, Y. H. (2014). Numerical simulation on fatigue crack growth of orthotropic steel highway bridge deck. *Journal of Vibration and Shock*, 33(14), 40–47.
25. Mustafa, A., Mohammad, A. E., Shota, U. (2012). Modelling and fatigue life assessment of orthotropic bridge deck details using FEM. *International Journal of Fatigue*, 40(6), 129–142. DOI 10.1016/j.ijfatigue.2011.12.015.